Geotech Geol Eng (2022) 40:4539–4549
https://doi.org/10.1007/s10706-022-02169-8

ORIGINAL PAPER

Research on the Evolution Mechanism of Water Inrush in Karst Tunnel and the Safety Thickness of Water-Resisting Rock Mass

Meixia Wang · Weimin Yang · Zongqing Zhou · Liping Li · Dunyi Deng · Qiwen Zhou

Received: 8 July 2021 / Accepted: 4 May 2022 / Published online: 1 August 2022

Abstract Water inrush due to rock mass progressive failure in karst tunnels is one of the disasters in tunnel construction. The practical measures to ensure the safety of tunnel construction are to clarify the mechanism of water inrush and reserve the safety thickness. In this paper, the geomechanical model test and numerical simulation were carried out based on the Xiema Tunnel in Chongqing, China. The results of the displacement and hydraulic pressure of the monitoring points in the physical and numerical models were analyzed. In view of the reserved safety thickness between the tunnel face and the water-filled karst cave, the orthogonal numerical simulation tests were designed considering the influence of the tunnel diameter, the cave diameter, the cave water pressure, and the surrounding rock grade. The influence laws and response sensitivity of each factor on the safety thickness were obtained. According to the numerical simulation results and the multiple linear regression method, the formula of safety thickness was derived. Finally, some measures and suggestions for preventing and controlling water inrush disasters were obtained.

Keywords Water inrush · Karst cave · Safety thickness · Numerical simulation

M. Wang · W. Yang (✉) · Z. Zhou · L. Li
Geotechnical and Structural Engineering Research Center, Shandong University, Jinan 250061, Shandong, China
e-mail: weimin.yang@sdu.edu.cn

Z. Zhou
e-mail: zongqing.zhou@sdu.edu.cn

W. Yang · Z. Zhou · L. Li
School of Qilu Transportation, Shandong University, Jinan 250061, Shandong, China
e-mail: zongqing.zhou@sdu.edu.cn

D. Deng · Q. Zhou
Shandong Highway Engineering Technology Research Center Co. Ltd, Jinan 250200, Shandong, China

1 Introduction

China is one of the countries with the enormous scale and number of tunnel construction (Qian and Lin 2016; Liu et al. 2021; Chen et al. 2020). In the process of tunnel excavation, major geological disasters such as large deformation, collapse, rock burst, and water inrush are often encountered (Zhang et al. 2021; Chen et al. 2021; Hencher 2019; Ariani et al. 2017; Naji et al. 2019; Rehbock and Jesel 2018; Panthi 2012; Li et al. 2020a; Vietthuc 2016). According to statistics, nearly 80% of the major disasters that occurred in the past decade are caused by water inrush. Water inrush causes not only serious casualties and economic losses but also brings serious challenges to the ecological environment and the utilization of groundwater resources (Wang et al. 2019; Li and Yang 2018; Hao et al. 2018). Due to the complexity and variability of geological conditions, water inrush is a dynamic destruction process that changes

with time, and it is affected by geological and engineering factors such as stratum lithology, geological structure, hydrogeological conditions, in-situ stress conditions, and construction methods. The process of water inrush can be briefly summarized as follows: under the influence of tunnel excavation, the equilibrium state of the stress field of surrounding rock mass and the seepage field of underground water changes drastically, and the energy accumulated in the groundwater is released instantaneously, which exceeds the strength of the water-resistance rock mass. The water flows to the excavation face at high speed, leading to water inrush (Gao et al. 2021; Xue et al. 2021; Hao et al. 2020; Zhou et al. 2021). Therefore, it is of great significance to clarify the mechanism of water inrush and reserve a certain thickness of water-resistance rock mass to prevent water inrush.

The determination of the safety thickness of water-resistance rock mass has attracted great attention, and extensive research has been carried out. At first, the empirical method, expert evaluation method, and engineering analogy method were used to analyze the safety thickness (Gan et al. 2007). A large number of mechanical models have been developed to obtain the safety thickness based on the elastic theory, elastic–plastic theory, limit analysis theory, fracture theory, and catastrophe theory (Guo et al. 2011; Yang and Zhang 2016; Li et al. 2014). At present, numerical simulations and physical model tests are used to study the safety thickness. The study on the safety thickness has gone through a process from qualitative analysis to semi-quantitative calculation and then to qualitative calculation. Jiang et al. (2017) carried out a series of large-scale geomechanical model tests to obtain minimum safety thickness. The results show that minimum safety thickness decreased with the increase of hydraulic pressure and increased with the increase of strata pressure. Besides, the two main destruction characteristics on the tunnel face for the water inrush disaster were analyzed. Liu et al. (2020a) obtained a critical safety thickness to prevent water inrush. The results show that the evolution of water inrush was significant and unstable when the safety thickness was smaller than the critical value. Li et al. (2020b) used the COMSOL Multiphysics software to simulate the process of water inrush, and the safety thickness was obtained by the multiple linear regression method. Xu et al. (2018) analyzed the mechanical mechanism of water inrush by the theory of elastic mechanics. According to the bending strength and shear strength of the rock mass, a semi-quantitative analytical method for calculating the minimum safety thickness of water-resistance rock mass was obtained. Liu et al. (2020b) used a water and mud inrush model for the nonlinear flow and mass transfer behavior to evaluate the safety thickness. And field studies with twenty-five grouting cycles and excavations were conducted to investigate the adequate safety thickness. Liu et al. (2020c) obtained the analytical solution of the critical safety thickness based on the upper bound theorem of limit analysis. The effects of rock mass parameters, karst cave parameters, and geometric parameters on the critical safety thickness were analyzed. Li et al. (2015a, b) proposed a simplified analytical method to determine the minimum safety thickness of water and mud inrush induced by filled-type karst. The results calculated by the proposed method are in good agreement with numerical simulations. However, there are few studies on the safety thickness of water-filled karst caves in front of the tunnel face under the comprehensive influence of multiple factors.

In this paper, the model test and numerical simulation research on the surrounding rock stability under the effect of water-filled karst caves were carried out. The mechanism of water inrush was analyzed. Numerical models were established based on the engineering background of the Xiema Tunnel. The orthogonal numerical simulation tests were designed considering the influence of the tunnel diameter, the cave diameter, the cave water pressure, and the surrounding rock grade on the safety thickness. Taking the penetration of the plastic zone as the failure criterion, the influence laws of each factor on the safety thickness were obtained, and the formula of safety thickness was derived by the multiple linear regression method. The research results play a guiding role in the prevention and control of water inrush disasters.

2 Engineering Background and Physical Model Test

Xiema Tunnel is located in Chongqing, China, with a maximum buried depth of 392 m and a length of 4200 m. The rock mass is mostly limestone. The physical and mechanical parameters were obtained in

consideration of the results of the laboratory tests and the related geological exploration data. The compression strength, elasticity modulus, friction angle, Poisson's ratio, cohesion, hydraulic conductivity, and density are 29.8 MPa, 59.5 GPa, 37.5°, 0.28, 4.30 MPa, 2.16×10^{-5}, and 2.65 g/cm^3, respectively. There are irregular karst caves and abundant groundwater in the tunnel site. Water inrush disasters occurred during the tunnel construction, and the water pressure was 0.4–0.6 MPa. To study the stability of the surrounding rock under the effect of a karst cave, a water inrush model test was carried out (Li et al. 2019). The size of the testing sample was 1.5 m in length, 1.0 m in width, and 1.0 m in height. The compression strength, elasticity modulus, friction angle, Poisson's ratio, cohesion, hydraulic conductivity, and density of the similar materials was 0.41 MPa, 0.8 GPa, 36°, 0.30, 0.06 MPa, 2.45×10^{-6} cm/s, and 2.51 g/cm^3, respectively. According to the geological survey report and the similarity ratio of the model test, the in-situ stress was 0.11 MPa. The monitoring elements were buried in essential locations to obtain the water pressure and displacement information. The design of the monitoring sections is as shown in Fig. 1. In the initial excavation step, the excavation length was 3 cm. When approaching the cave, the distance became 1.5 cm (Yang et al. 2019).

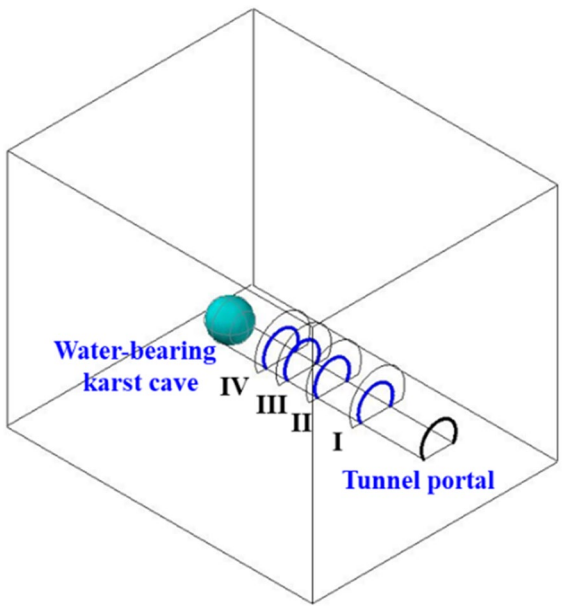

Fig. 1 Design of the monitoring sections

3 Numerical Simulation

3.1 Boundary Conditions and Numerical Simulation Procedure

The finite element method software COMSOL Multiphysics was used to simulate the geomechanical model test and obtain variations of physical and mechanical information such as the displacement, stress, and seepage pressure of the surrounding rock mass under the influence of high in situ stress and water-rich karst cave. The solid mechanics module and Darcy's law module in the COMSOL Multiphysics software were used to perform fluid–solid coupling analysis. As shown in Fig. 2, the size of the numerical model was the same as that of the model test. The longitudinal direction of the tunnel was the X-axis, the vertical direction was the Z-axis, and the direction perpendicular to the XZ plane was the Y-axis. The origin was at the front perspective point at the bottom of the model. The numerical model was meshed by 17,106 tetrahedral elements.

The surrounding rock mass was assumed to be homogeneous, isotropic, incompressible solid. It was governed by an elastic–plastic constitutive model based on the Mohr–Coulomb criterion. And the fluid was assumed to be an isotropic steady seepage model. Ignoring the deformation caused by temperature changes, it is considered that the seepage field is in

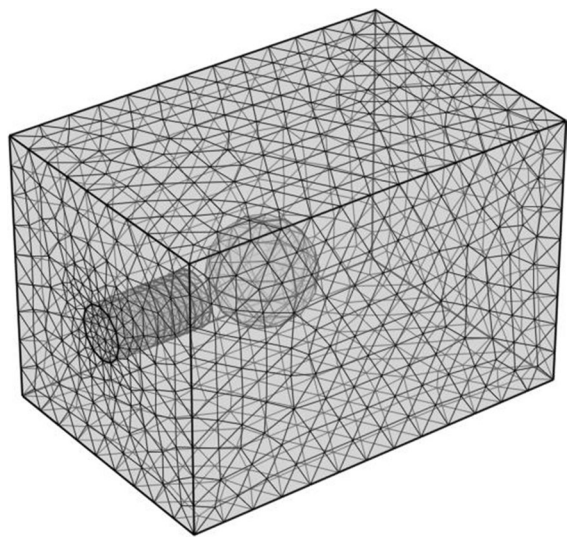

Fig. 2 Numerical model

an isothermal state. In the numerical simulation, the bottom of the model was fixed in all directions. The top and sidewalls of the numerical model were free to move under the applied loading. The hydraulic boundary condition at the top, bottom, and side surfaces were all free. Meanwhile, the tunnel face was also free. The water pressure of the karst cave was 10 kPa. The physical and mechanical parameters of the surrounding rock mass in the numerical simulation were consistent with those in the model test. The density and viscosity coefficient of the water was 1000 kg/m^3 and 1.005×10^{-3} Pa s, respectively.

The initial crustal stress includes the horizontal crustal stress caused by the model deformation and the vertical crustal stress caused by the self-weight of the model. In the calculation process, the stress of the rock before the tunnel excavation was calculated firstly, then the elastic–plastic characteristics of the model after removing the rock mass inside the tunnel were calculated. The influence of lining was not considered during the excavation, and it was beneficial to analyze the evolution laws of the surrounding rock mass. Because of computational efficiency, the excavation length was 6 cm in the initial excavation step. When approaching the cave, the distance became 3 cm.

3.2 Numerical Analysis of the Excavation Process

Multiple calculation steps were set, each of which included a set of physical fields. At the beginning of each calculation step, the selection of the computational zone and parameters were carried out. The numerical simulation steps are as follows:

Step 1 Ground stress balance before tunnel excavation. The computational zone was the whole model.

Step 2 Simulation of the first excavation step. The calculation result of Step 1 was used as the initial value of Step 2, and the fluid–structure coupling physical field one was calculated. The length of excavation step 1 was 3 cm. The computational zone should delete the area where excavation step 1 was located.

Step 3 Simulation of the second excavation step. The calculation result of Step 2 was used as the initial value of Step 3, and the fluid–structure coupling physical field two was calculated. The computational zone should delete the area where excavation step 1 and step 2 were located.

Step 4 By analogy, the simulation of tunnel excavation was completed until all computational zone were deleted.

Figure 3 shows the displacement variations of surrounding rock mass during excavation. Owing to the impossibility of publishing the numerical example in the whole length and the difference of the programs, only the displacement programs of some excavation steps were listed. The displacement of the tunnel vault was downward, whereas the displacement of the tunnel floor was upward because of the combined action of ground stress and water pressure. As shown in

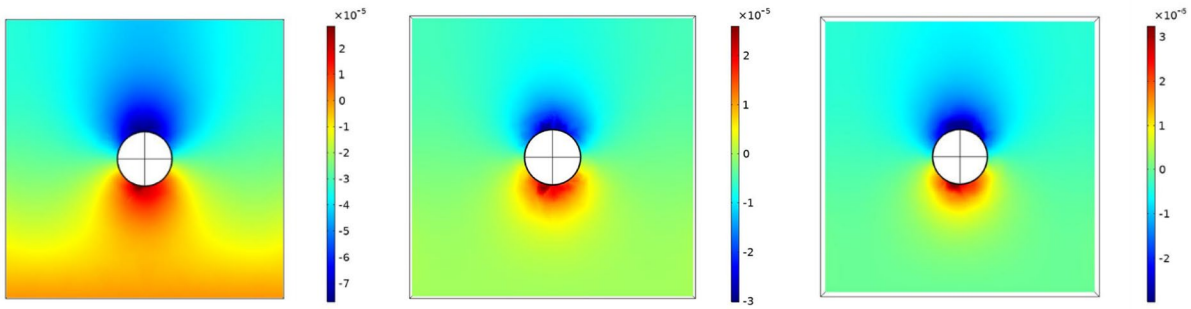

Fig. 3 Vertical displacement of tunnel face in numerical simulation (unit: m)

Fig. 4, the hydraulic pressure of the surrounding rock mass was symmetrically distributed. The hydraulic pressure value first increased and then decreased from the tunnel to the model boundary.

4 Analysis of the Results

Based on the results of the model test and numerical simulation, the vertical displacement variations at the monitoring points D_{10}, D_{13} of the monitoring section III and the seepage pressure variations at monitoring points H_2, H_4 of the monitoring sections II, III were analyzed. The monitoring points H_2 and H_4 were located in the center of the monitoring section. The monitoring point D_{10} was 200 mm above the section center, and the monitoring point D_{13} was 200 mm to the left of the section center.

4.1 Analysis of Displacement

Figure 5 shows the vertical and horizontal displacement of monitoring points D_{10} and D_{13} in numerical simulation and model test. It can be seen that the variation trend of vertical and horizontal displacement of the surrounding rock was consistent between the numerical simulation and model test. However, the displacement value of the numerical simulation was smaller than that of the model test. In the initial stage of tunnel excavation, the displacement increased slightly. The magnitude of the vertical and horizontal displacement increased sharply at the excavation step 6. This may be due to that the monitoring section was exposed (Li et al. 2019). As the distance between the tunnel face and the karst cave decreased, the displacement continued to increase under the influence of the water-filled cave. Meanwhile, it can be seen from Fig. 5 that the horizontal displacement was less than the vertical displacement. The excavation disturbed zone in the vertical direction was larger than that in the horizontal direction. When the section was excavated, timely support should be carried out. When the tunnel face was close to the karst cave, the surrounding rock monitoring should be strengthened, and reasonable and effective measures should be taken to prevent the surrounding rock from large deformation and water inrush.

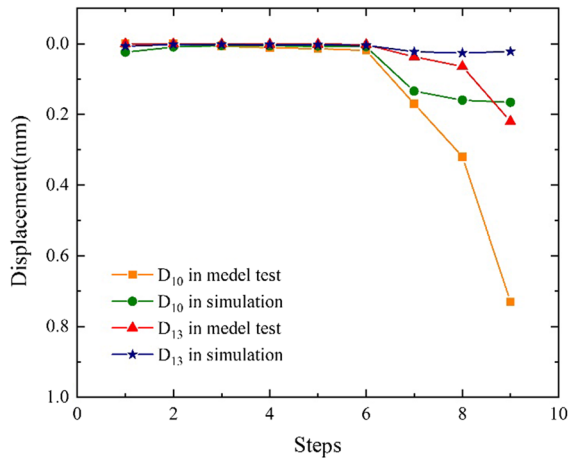

Fig. 5 Displacement of key monitoring points D_{10} and D_{13}

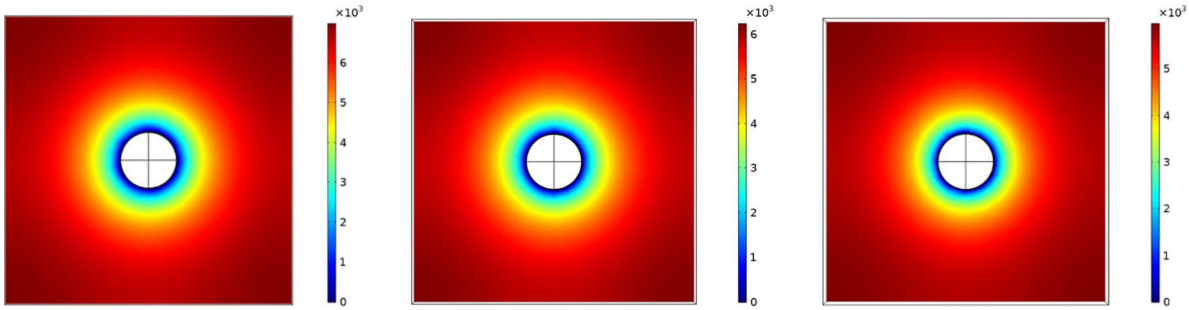

Fig. 4 Seepage pressure of tunnel face in numerical simulation (unit: Pa)

4.2 Analysis of Seepage Pressure

As shown in Fig. 6, the seepage pressure at monitoring points H_2 and H_4 decreased with the excavation step. There was generally a good agreement between the variation trend of the seepage pressure at the same point in the model test and the numerical simulation. The seepage pressure at the monitoring point H_2 gradually decreased with the excavation in the model test and the numerical simulation. For the monitoring point H_4, the seepage pressure increased slightly in the model test. Because the excavation disturbance of the tunnel caused stress redistribution in the surrounding rock mass. The rock mass began to deform under the redistribution stress, the water can be supplied by the karst cave in the initial stage, so the seepage pressure increased (Li et al. 2019). The seepage pressure at the monitoring point H_4 kept decreasing in the numerical simulation. Numerical simulations regard the water pressure as the boundary force acting on the element networks rather than the actual water. The decrease in seepage pressure led to the increase in seepage velocity. It was easier for groundwater to penetrate into the rock mass, resulting in a decrease of mechanical properties. Therefore, it is essential to strengthen the support measures to improve the stability of the surrounding rock mass.

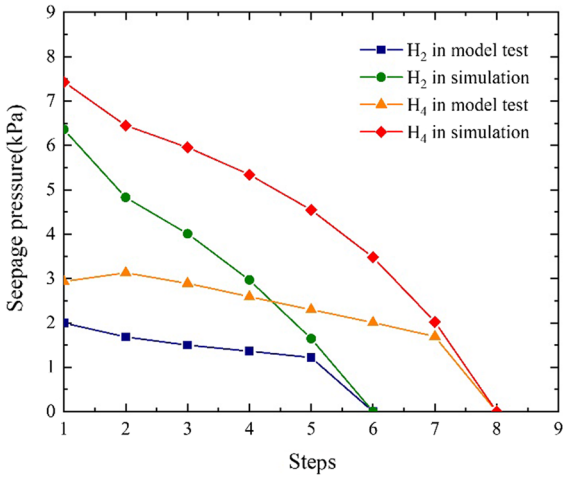

Fig. 6 Seepage pressure of monitoring points H_2 and H_4

5 Safety Thickness of Water Inrush

Water inrush is a dynamic damage phenomenon due to the rapid transformation of the rock conditions. Water flows from water-filled karst caves along the seepage channel, the water-resisting rock mass is broken, and water flows into the tunnel, resulting in water inrush. When the thickness between the tunnel face and the karst cave is less than the minimum safety thickness, water inrush will occur. Therefore, the safety thickness of water-resisting rock mass is an important guarantee to avoid water inrush disasters. This paper studies the influence of different factors on the minimum safety thickness based on the Xiema Tunnel. The model of the model test was enlarged according to the geometric similarity ratio. The safety thickness is the horizontal distance from the center point of the tunnel face to the karst cave when the plastic zone is connected.

5.1 Scheme of Numerical Simulation

To comprehensively study the influence of tunnel diameter, cave water pressure, surrounding rock grade, and cave diameter on the safety thickness of water-resisting rock mass, orthogonal tests were carried out. The orthogonal test plan was shown in Table 1. Each experimental factor had five levels. The tunnel diameter ranged from 4 to 12 m, increasing by 2 m at each level. The cave diameter was from 3 to 7 m, with an increase of 1 m per lever. The karst water pressure ranged from 2.0 to 4.0 MPa, with an increase of 0.5 MPa per lever. The surrounding rock grade was divided into five levels.

5.2 Analysis of Numerical Simulation

It can be seen from the simulation results that as the tunnel face gradually approached the karst cave, the plastic zone increased. At the same time, the plastic zone around the cave also expanded and finally connected with the plastic zone of the tunnel face. If the tunnel face continued to approach the water-filled karst cave, the plastic zone would further increase, resulting in water and mud disasters. The results of the safe thickness are shown in Table 2. According to the results, the range analysis was carried out to obtain the influence degree of each factor on the safety thickness, as shown in Table 3. It can be seen

Table 1 Orthogonal test plan

Number	Tunnel diameter (m)	Cave diameter (m)	Cave water pressure (MPa)	Surrounding rock grade
1	4	4	4	4
2	6	4	3.5	3
3	8	3	3.5	5
4	10	3	3	4
5	12	3	2.5	3
6	6	5	3	5
7	10	4	2.5	1
8	12	4	2	5
9	12	6	3.5	4
10	10	6	4	5
11	8	6	2	1
12	6	6	2.5	2
13	6	3	4	1
14	10	5	2	3
15	4	5	3.5	1
16	4	3	2	2
17	8	4	3	2
18	12	7	3	1
19	4	6	3	3
20	8	7	4	3
21	6	7	2	4
22	10	7	3.5	2
23	12	5	4	2
24	4	7	2.5	5
25	8	5	2.5	4

from the table that the surrounding rock mass grade had the most significant influence on the safety thickness of water-resisting rock mass, followed by the tunnel diameter, and cave water pressure had less effect on it.

5.2.1 Influence of Surrounding Rock Grade on Safety Thickness

Figure 7 shows the change curve of the safety thickness of the tunnel with the surrounding rock grade. It can be seen from the figure that the safety thickness increases with the improvement of the surrounding rock grade. The surrounding rock grade reflects the comprehensive physical and mechanical parameters of the surrounding rock mass. The lower the surrounding rock grade is, the lower the strength is, and the worse the self-stabilization ability. During the excavation, loosening, collapse, and penetration of the plastic zone are likely to occur. There is a linear relationship between the safety thickness (S) and the surrounding rock grade (G). The relationship can be expressed by Eq. (1), and the correlation coefficient is 0.993.

$$S = 5.746 + 0.0233G^{3.56} \quad (1)$$

Table 2 Results of the safe thickness

Number	Safety thickness (m)	Number	Safety thickness (m)
1	8.00	14	8.30
2	4.50	15	4.50
3	11.70	16	3.30
4	9.50	17	5.60
5	8.70	18	7.50
6	11.90	19	7.00
7	6.20	20	7.80
8	14.30	21	7.60
9	11.50	22	8.90
10	14.60	23	7.50
11	5.50	24	12.50
12	5.00	25	6.90
13	4.30		

Table 3 Range analysis

Item	Tunnel diameter (m)	Cave diameter (m)	Cave water pressure (MPa)	Surrounding rock grade
K_1	35.3	37.5	39.0	28
K_2	33.3	38.6	39.3	30.3
K_3	37.5	39.1	41.5	36.3
K_4	47.5	43.6	41.1	43.5
K_5	49.5	44.3	42.2	65.0
k_1	7.06	7.50	7.80	5.60
k_2	6.66	7.72	7.86	6.06
k_3	7.50	7.82	8.30	7.26
k_4	9.50	8.72	8.22	8.70
k_5	9.90	8.86	8.44	13.00
R	16.2	6.8	3.2	37

K_j is the sum of indicators, k_j is the average value, R is the range

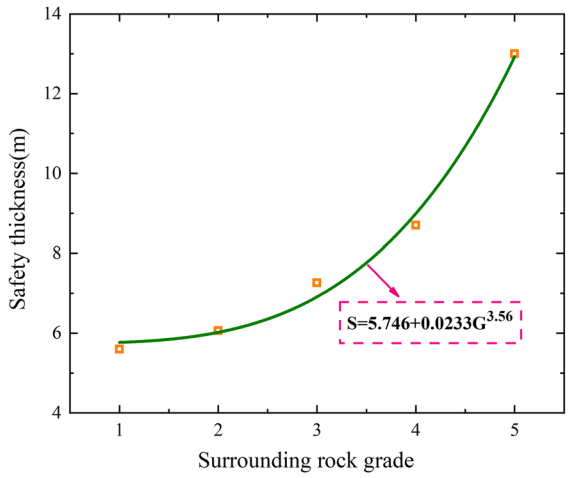

Fig. 7 The relationship between the safety thickness and the surrounding rock grade

5.2.2 *Influence of Cave Water Pressure on Safety Thickness*

It can be seen from Fig. 8 that when other factors remain unchanged, increasing the cave water pressure will increase the safety thickness. The increase rate is low. However, when the water pressure of the karst cave is more ten 10 MPa, it will have a great influence on the safety of tunnel construction. The relationship between the safety thickness (S) and the water pressure (P) can be expressed by Eq. (2), and the correlation coefficient reaches 0.859.

$$S = 3.455\ln(P+7.524) \tag{2}$$

5.2.3 *Influence of Cave Diameter on Safety Thickness*

Figure 9 shows the change curve of the safety thickness with the cave diameter. The safety thickness of the water-resisting rock mass increases as the cave diameter increases. The increase in the cave diameter makes the total water pressure borne by the rock mass between the tunnel face and the karst cave increase, which is more unfavorable to the stability of the rock mass. Therefore, the safety thickness of the water-resisting rock mass increases. The relationship between the safety thickness (S) and the cave diameter (C_d) can be expressed by Eq. (3), and the correlation coefficient reaches 0.90.

$$S = 6.264 + 0.372C_d \tag{3}$$

5.2.4 *Influence of Tunnel Diameter on Safety Thickness*

With the increase of tunnel diameter, the safety thickness of the water-resisting rock mass increases, and

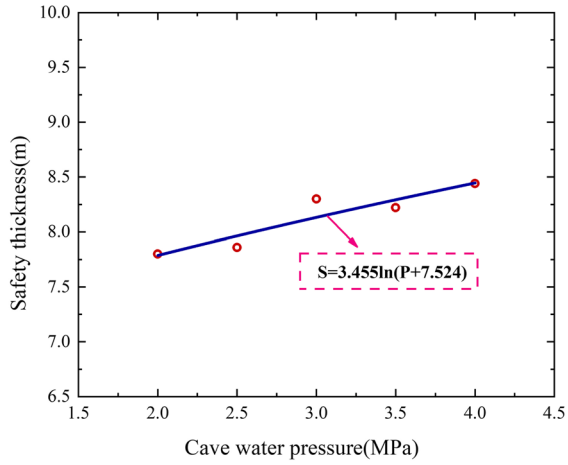

Fig. 8 The relationship between the safety thickness and the cave water pressure

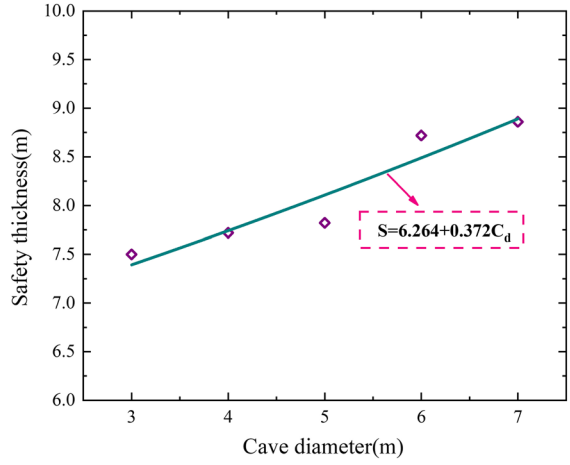

Fig. 9 The relationship between the safety thickness and the cave diameter

there is an exponential function relationship between them, as shown in Fig. 10. The effect of tunnel diameter on safety thickness is inferior to that of surrounding rock grade. After fitting, the relationship between the safety thickness (S) and the tunnel diameter (T_D) can be expressed by Eq. (4), and the correlation coefficient reaches 0.888.

$$S = 6.456+0.008T_D^{2.468} \tag{4}$$

5.3 Safety Thickness Prediction Model

A multiple linear regression equation is a linear combination based on the basic regression equations of different independent and dependent variables. The regression equation with the largest correlation coefficient of each variable and the dependent variable is selected as the basic regression equation. The formula parameters are estimated by the ordinary least squares. Based on the analysis, its multiple regression equation is as follows:

$$S = -0.011G^{3.56}-14.554\ln(P+7.524)-0.358C_d + 0.025T_D^{2.468}+40.117$$

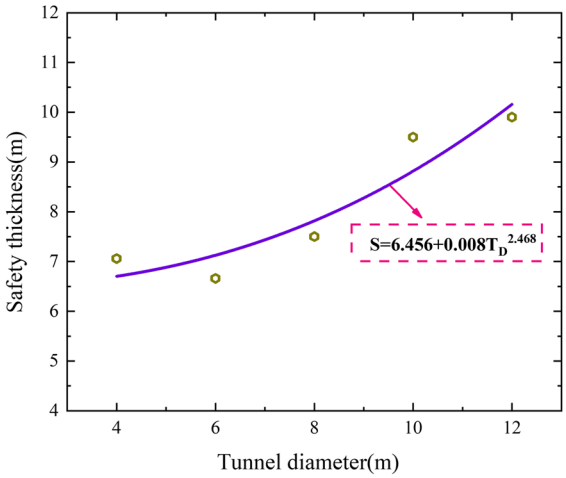

Fig. 10 The relationship between the safety thickness and the tunnel diameter

6 Prevention and Control Measures of Water Inrush in Karst Tunnels

The prevention and control of water inrush disasters is the key to the safe construction of karst tunnels.

Scientific, effective, safe, and economic prevention and control measures should be made according to the size and occurrence characteristics of the karst cave. Based on the results of model tests and numerical simulations, the prevention and control measures of water inrush disasters in karst tunnels are analyzed comprehensively, which can be summarized as follows:

(1) Route selection to avoid karst caves. According to the numerical simulations, when the distance between the karst cave and the tunnel exceeds the safety thickness, the risk of water inrush disasters during tunnel construction is extremely low. Therefore, when the karst caves are identified in advance by geological prediction, especially for large karst caves with complex conditions, the excavation route should avoid karst caves. The typical water inrush case corresponding to prevention and control measure of the route selection is Yesanguan Tunnel, China (Li et al. 2020a, b, c).

(2) Drainage and pressure relief. This measure is mainly aimed at high-pressure karst caves. Drainage flumes and pumps are used to divert water from the karst caves to the outside of the tunnel, thereby reducing the water pressure in the cave. Although the numerical simulation results show that the effect of water pressure on the safety thickness is not apparent, for high-pressure caves, this measure has a significant impact on reducing the risk of water inrush. Moreover, for a single cave that is not connected to other water-bearing structures, draining the water in the karst cave is an effective measure to avoid human casualties caused by water inrush. The typical water inrush case corresponding to prevention and control measure of the drainage and pressure relief is Maluqing Tunnel, China (Huang et al. 2011).

(3) Grouting reinforcement. Grouting is one of the most widely used measures in the prevention and control of water inrush. Pre-grouting can improve the mechanical properties of surrounding rock and reduce the permeability coefficient to prevent water inrush. The typical water inrush case corresponding to prevention and control measure of the grouting

reinforcement is Yuanliangshan Tunnel, China (Li et al. 2015a, b).

In addition, water inrush disaster prevention and control should be combined with tunnel construction advanced geological prediction, monitoring and early warning. Various measures are implemented together to ensure the safety of tunnel construction.

7 Conclusions

In this paper, the mechanism of water inrush due to rock mass progressive failure in karst tunnels was studied by model tests and numerical simulations. And the safety thickness between the tunnel face and the water-filled karst cave was analyzed. The following conclusions are summarized.

(1) As the distance between the tunnel face and the karst cave decreases, the displacement continues to increase under the influence of the water-filled cave. The excavation disturbed zone in the vertical direction is more significant than that in the horizontal direction. The seepage pressure decreases with the excavation step. The displacement deformation changes the porosity of the surrounding rock mass, and the seepage pressure changes accordingly. The change rule of the seepage pressure and displacement can give an understanding of the mechanism of water inrush.

(2) To obtain the influence laws and response sensitivity of tunnel diameter, cave diameter, cave water pressure, and surrounding rock grade on the safety thickness, orthogonal numerical simulation tests are designed. The results show that the surrounding rock mass grade has the greatest influence on the safety thickness, followed by the tunnel diameter, and cave water pressure has less effect on it. According to the multiple linear regression analysis, the formula of the reserved safety thickness is obtained: $S = -0.011G^{3.56} - 14.554\ln(P+7.524) - 0.358C_d + 0.025T_D^{2.468} + 40.117$. This formula can be used to guide the tunnel construction in karst areas.

(3) The prevention and control of water inrush disasters is the key to the safe construction of karst tunnels. According to the results of numerical simulation and model test, the prevention and control measures of water inrush disasters are comprehensively analyzed, which mainly include: route selection to avoid karst caves, drainage and pressure relief, and grouting reinforcement. In the actual project, reasonable, economical, safe, and efficient water inrush prevention and control measures should be selected according to actual conditions. The results can provide guidance for tunnel projects with similar engineering conditions. The safe construction of the tunnel can be guaranteed.

Acknowledgements Much of the work presented in this paper was supported by the National Natural Science Foundation of China (51879148, 51991391, U1806226), the Key Technology Research and Development Program of Shandong (2019GSF111030).

Author Contributions All authors contributed to the study conception and design. MW: Material preparation, Data collection, Writing Original Draft. WY: Project administration, Funding acquisition. ZZ: Resources, Supervision, Writing—Review and Editing. LL: Conceptualization, Methodology. DD: Formal analysis, QZ: Validation, Data Curation.

Data Availability The datasets generated during and/or analyzed during the current study are available from the corresponding author on reasonable request.

Code Availability All code generated or used during the study are proprietary or confidential in nature and may only be provided with restrictions.

Declarations

Conflict of interest We declared that we have no financial and personal relationships with other people or organizations that can inappropriately influence our work.

References

Ariani F, Baldasseroni A, Muller A, Biffino M, Matteucci A (2017) Reduction of excavation face collapse risk in tunneling. Med Lav 108:446–454

Chen ZY, Zhang YP, Li JB, Li X, Jing LJ (2021) Diagnosing tunnel collapse sections based on TBM tunneling big data and deep learning: a case study on the Yinsong Project, China. Tunn Undergr Sp Tech 108:103700

Chen JX, Xu ZL, Luo YB, Song JK, Liu WW, Dong FF (2020) Application of the upper-bench CD method in super large-span and shallow tunnel: a case study of Letuan Tunnel. Adv Civ Eng 2020:1–16

Gan KR, Yang Y, Li JS (2007) Analysis on karst water inflow mechanism and determination of thickness of safe rock

walls: case study on a tunnel. Tunn Constr 27(3):13–16 (**in Chinese**)

Gao CL, Li LP, Zhou ZQ, Li ZH, Cheng S, Wang LG, Zhang DS (2021) Peridynamics simulation of water inrush channels evolution process due to rock mass progressive failure in karst tunnels. Int J Geomech 21(4):04021028

Guo JQ, Ren LW, Liu XL (2011) Study on safe thickness of comparatively intact rock ahead of karst tunnel face. Appl Mech Mater 90–93:2456–2459

Hao YQ, Rong XL, Lu H, Xiong ZM, Dong X (2018) Quantification of margins and uncertainties for the risk of water inrush in a karst tunnel: representations of epistemic uncertainty with probability. Arab J Sci Eng 43(4):1627–1640

Hao YQ, Lu H, Shi YH, Geng H, Xi J, Feng SF (2020) Uncertainty evaluation of water inrush in karst tunnels based on epistemic uncertainty with possibility theory. Math Probl Eng 2020:1–12

Hencher SR (2019) The glendoe tunnel collapse in Scotland. Rock Mech Rock Eng 52(10):4033–4055

Huang M, Zhang XD, Xu MK, Cai LQ (2011) Mechanism analysis and criterion for avoiding risk of karst water burst flood illustrated in Maluqing Tunnel. Adv Mater 250–253:2650–2661

Jiang HM, Li L, Rong XL, Wang MY, Xia YP, Zhang ZC (2017) Model test to investigate waterproof-resistant slab minimum safety thickness for water inrush geohazards. Tunn Undergr Sp Tech 62:35–42

Li TZ, Yang XL (2018) Risk assessment model for water and mud inrush in deep and long tunnels based on normal grey cloud clustering method. KSCE J Civ Eng 22(5):1991–2001

Li J, Lu H, Xia YP (2014) Survey and research on estimation method of against-inrush safe thickness of rock strata in karst tunnels. Tunn Constr 34(9):862–872 (**in Chinese**)

Li LP, Lei T, Li SC, Xu ZH, Xue YG, Shi SS (2015a) Dynamic risk assessment of water inrush in tunnelling and software development. Geomech Eng 9(1):57–81

Li SC, Lin P, Xu ZH, Li LP, Guo M, Sun CQ, Wang J, Song SG (2015b) Minimum safety thickness of water and mud inrush induced by filled-type karst water bearing structures based on theory of slice method. Rock Soil Mech 36(7):1989–1994 (**in Chinese**)

Li SC, Gao CL, Zhou ZQ, Li LP, Wang MX, Yuan YC, Wang J (2019) Analysis on the precursor information of water inrush in karst tunnels: a true triaxial model test study. Rock Mech Rock Eng 52:373–384

Li LP, Sun SQ, Wang J, Yang WM, Song SG, Fang ZD (2020a) Experimental study of the precursor information of the water inrush in shield tunnels due to the proximity of a water-filled cave. Int J Rock Mech Min 130:104320

Li LP, Xiong YF, Wang J, Gao XC, Wang K, Sun HC, Fang ZD (2020b) Comprehensive influence analysis of multiple parameters on the safety thickness against water inrush in shield tunnel. Int J Geomech 20(12):04020226

Li ZY, Wang YC, Olgun CG, Yang SQ, Jiao QL, Wang MT (2020c) Risk assessment of water inrush caused by karst cave in tunnels based on reliability and GA-BP neural network. Geomat Nat Haz Risk 11(1):1212–1232

Liu JQ, Chen WZ, Deng ZP, Liu TG, Dong JL (2020a) Impacts of confining pressure and safety thickness on water and mud inrush in weathered granite. Mar Georesour Geotech 38(2):144–153

Liu JQ, Chen WZ, Yuan KV, Zhou XS (2020b) Groundwater-mud control and safety thickness of curtain grouting for the Junchang Tunnel: a case study. Tunn Undergr Sp Tech 103:103429

Liu QW, Sun SQ, Wang HB, Dong JX, Hu HC (2020c) A calculation method for safety distance between the confined karst cave and the shield tunnel based on upper bound theorem. Geotech Geol Eng 38(6):6587–6599

Liu WW, Chen JX, Luo YB, Shi Z, Wu YF (2021) Deformation behaviors and mechanical mechanisms of double primary linings for large-span tunnels in squeezing rock: a case study. Rock Mech Rock Eng 54(5):2291–2310

Naji AM, Emad MZ, Rehman H, Yoo H (2019) Geological and geomechanical heterogeneity in deep hydropower tunnels: a rock burst failure case study. Tunn Undergr Sp Tech 84:507–521

Panthi KK (2012) Evaluation of rock bursting phenomena in a tunnel in the Himalayas. B Eng Geol Environ 71(4):761–769

Qian QH, Lin P (2016) Safety risk management of underground engineering in China: progress, challenges and strategies. J Rock Mech Geotech 8(4):423–442

Rehbock SM, Jesel T (2018) Fault induced rock bursts and micro-tremors–experiences from the gotthard base tunnel. Tunn Undergr Sp Tech 81:358–366

Vietthuc C (2016) Mechanism on water inrush disaster of filling karst piping and numerical analysis of evolutionary process in highway tunnel. J Cent South Univ 47(12):4173–4180

Wang XT, Li SC, Xu ZH, Hu J, Pan DD, Xue YG (2019) Risk assessment of water inrush in karst tunnels excavation based on normal cloud model. B Eng Geol Environ 78(5):3783–3798

Xu ZH, Wu J, Li SC, Zhang B, Huang X (2018) Semianalytical solution to determine minimum safety thickness of rock resisting water inrush from filling-type karst caves. Int J Geomech 18(2):04017152

Xue YG, Kong FM, Qiu DH, Su MX, Zhao Y, Zhang K (2021) The classifications of water and mud/rock inrush hazard: a review and update. B Eng Geol Environ 80(3):1907–1925

Yang ZH, Zhang JH (2016) Minimum safe thickness of rock plug in karst tunnel according to upper bound theorem. J Cent South Univ 23(9):2346–2353

Yang WM, Wang MX, Zhou ZQ, Li LP, Yuan YC, Gao CL (2019) A true triaxial geomechanical model test apparatus for studying the precursory information of water inrush from impermeable rock mass failure. Tunn Undergr Sp Tech 93:103078

Zhang J, Wang MX, Xi CH (2021) Tunnel collapse mechanism and its control strategy in fault fracture zone. Shock Vib 2021:1–10

Zhou ZQ, Li ZH, Gao CL, Zhang DS, Meixia W, Wei CC (2021) Peridynamic micro-elastoplastic constitutive model and its application in the failure analysis of rock masses. Comput Geotech 132:104037